



Aggregated wind power characteristic curves and artificial intelligence for the regional wind power infeed estimation

Yang Li¹ · Przemysław Janik² · Harald Schwarz¹

Received: 21 October 2022 / Accepted: 19 August 2023 / Published online: 11 September 2023
© The Author(s) 2023

Abstract

The wind power generation is highly dependent on current weather conditions. In the course of the energy transition, the generation levels from volatile wind energy are constantly increasing. Accordingly, the prediction of regional wind power generation is a particularly important and challenging task due to the highly distributed installations. This paper presents a study on the role of regional wind power infeed estimation and proposes a multi-aggregated wind power characteristics model based on three scaled Gumbel distribution functions. Multi-levels of wind turbines and their allocation are investigated for the regional aggregated wind power. Relative peak power performance and full load hours are compared for the proposed model and the real measurement obtained from a local distribution system operator. Furthermore, artificial intelligence technologies using neural networks, such as Long Short-Term Memory (LSTM), stacked LSTM and CNN–LSTM, are investigated by using different historical measurement as input data. The results show that the suggested stacked LSTM performs stably and reliably in regional power prediction.

Keywords Artificial intelligence · Aggregated wind power characteristics · Regional wind power

1 Introduction

The Renewable Energy Act (EEG, German: Erneuerbare-Energien-Gesetz) in Germany indeed accelerates the investment in renewable energies (RE) in the power system. The installed capacity of RE has increased from around 10 GW in 2000 to about 132 GW in 2020 [1]. The share of RE in gross electricity consumption has also risen, from 6% in 2000 to 45.3% in 2020 [1]. However, the inherent uncertainty of the renewable energy increases the instability of the power grid system and endanger it with grid congestion. The delayed grid network extension makes it impossible for the grid system to absorb such a large amount of intermittent RE power. To address this, curtailing overproduction of RE electricity

has become a necessary measure to prevent grid overloading [2]. Within the framework of the feed-in management in Germany, approx. 6 million euros were paid for the measure compensation in 2009 and this value rose to around 760 million euros in 2020 for 6,146 GWh curtailed renewable energy [3]. Approx. 96.7% of the curtailed energy are from wind energy source [3].

Therefore, a lot of effort in power estimation and prediction, especially for wind power generation, has been carried out by researchers in recent years. Wind energy exhibits temporal uncertainty and spatial variability due to geographical and meteorological conditions [4]. Generally, wind power prediction methods can be categorized into two approaches, the physical approach and the data-driven approach [5–8]. The physical approach is based on analysing the physical model of the wind power transformation process. The wind power can be calculated by using numerical weather prediction (NWP) data. While this approach can achieve a good prediction performance for a single wind turbine (WT), its utilization is limited due to large amount of calculation and the unsatisfactory short-term prediction accuracy [9, 10]. Therefore, purely relying on physical methods has not been widely used in the field of regional wind power prediction.

✉ Yang Li
liyang@b-tu.de

¹ Department of Energy Distribution and High Voltage Engineering, Brandenburg University of Technology Cottbus-Senftenberg, Siemens-Halske-Ring 13, 03046 Cottbus, Germany

² Department of Electrical Engineering Fundamentals, Wrocław University of Science and Technology, 50-377, Wrocław, Poland

Data-driven statistical method refers to the utilization of historical wind power data to generate predictions, such as autoregressive moving average (ARMA) [11] and autoregressive integrated moving average (ARIMA) [12], which exhibit adeptness in modelling linear relationships between historical and future data [10, 13]. However, their ability to handle nonlinear data is still insufficient, resulting in limited fitting performance [13, 14].

The data-driven method based on artificial intelligence (AI) can avoid the detailed physical transformation process [15]. The historical measured power data and meteorological data can be utilized as input features. Artificial neural networks are employed to capture the internal mapping relationships between the input features and output values. In recent years, there has been extensive research conducted in the field of power prediction, with a particular focus on deep learning techniques. Among these techniques, the Long Short-Term Memory (LSTM) has emerged as a popular choice for various prediction tasks. In a study referenced as [16], the authors demonstrate that the use of LSTM leads to a further reduction in PV power prediction error compared to the alternative methods. A study in reference [17] proved that LSTM can achieve excellent performance in wind power prediction. It highlighted LSTM's remarkable ability to learn features from sequence data, particularly when applied to wind datasets. LSTM, as a type of recurrent neural network, is specifically designed for processing data with time series features [16, 17]. LSTM can remember and connect the previous information to the presented obtained data [17]. The inclusion of a forget gate in LSTM address the vanishing and exploding gradient problem commonly encountered in RNN [17]. Compared with the traditional neural network, deep learning methods have the capability to extract and discover higher-level features from the raw input data. Additionally, combined models such as CNN–LSTM have been successfully applied in wind power prediction and show a good performance [6, 7, 18–20]. These studies usually focus on power prediction for individual wind turbines or wind farms within a specific area. However, power grid operation and scheduling does not focus on the power generation performance of an individual wind turbine, instead, it requires a holistic assessment of the overall power generation within a specific region [21].

In order to obtain the regional large-scale wind power, it is necessary to aggregate the individual power curves from each wind turbine (WT). Nevertheless, it is not feasible due to the significant computational requirements and lack of characteristic data for each WT. To address this challenge, the representative power curves from measured reference power plants are used to calculate the power output of unknown power plants. This approach has been successfully applied

in up-scaling the regional power prediction in both photovoltaic (PV) and wind [22, 23]. Indeed, the reference plants ultimately has a great influence on the prediction results.

The main issue is how to fit temporal and spatial features for the regional wind power prediction. Therefore, in this paper, we propose a novel method for regional wind power prediction that leverages both physical process of wind power generation and the statistical characteristic curves of wind turbines (WTs). We classify wind turbines based on their installed capacity and commissioning date. With the help of the proposed aggregated regional power curves the regional wind power is to be achieved. The regional wind power represents the aggregated power generated by distributed WT generators and supplied to the local electricity grid network. In addition, we employ AI deep learning models, including LSTM, stacked LSTM and CNN–LSTM, to extract the relationship between regional measured wind speeds from different measurement sites and wind power. By exploring different historical measurement sizes, we aim to improve the accuracy of the current regional aggregated wind power estimation.

The contributions of this paper lie in providing a method that enables accurate regional wind power prediction, essential for efficient grid operation and scheduling. The successful implementation of the proposed method can have significant engineering implications, enhancing grid stability and facilitating the integration of renewable energy sources into the power system.

The roadmap of this work is constructed as follows: Section Methodology defines the proposed model including aggregated power characteristic and AI models. Section Results and Discussion illustrate the case study results and performance evaluation. Finally, we give the conclusion of the study.

2 Methodology

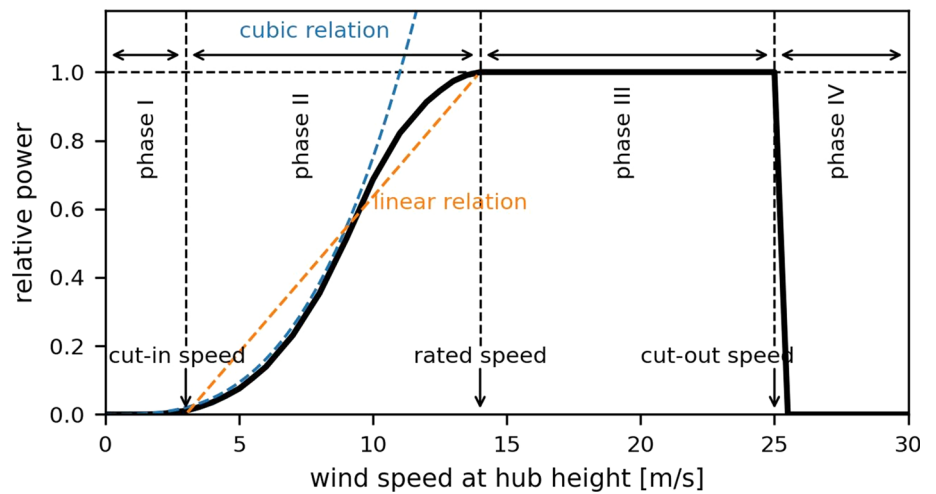
2.1 Aggregated regional wind power model

2.1.1 Wind power output characteristic

The power output characteristic (i.e. performance curve) of WT describes the relationship between the wind speed at the hub height and the electrical power delivered by the generator. A typical power characteristic curve of a single wind turbine is shown in Fig. 1. The wind power performance curve can be divided into four phases according to its operating features [24].

In phase I, the wind speed is below the minimum cut-in speed of a wind turbine. To enable operation of the wind turbine, a minimum wind energy is required to compensate for friction and inertial forces of the turbine. Therefore, no

Fig. 1 A typical power characteristic curve of one single wind turbine generator



electrical power is generated in phase I, and the turbine does not start.

In phase II, at a cut-in wind speed of approx. 2–4 m/s, the wind turbine is switched on to convert the wind energy into electrical energy. The power output increases with the wind speed. The rated wind power is reached at the turbine-specific rated wind speed, typically around 12–15 m/s. In addition, the power output in phase II can be simplified as linear relation [25]. The power curve of wind turbines is theoretically described by the 3rd power (cubic function) of the wind speed at hub height. The maximum power that can be extracted from the wind energy is derived from Betz’s law [24, 26]. A power coefficient c_p is defined, which represents the ratio of the power extracted from the wind to the wind turbine power output. It can be described in the following equation:

$$P_{WT} = \frac{1}{2} * c_p * \rho_{air} * A_{rotor} * v_h^3 \tag{1}$$

where P_{WT} is wind turbine generator power output, c_p is the power coefficient, ρ_{air} is air density, A_{rotor} is the rotor swept area, v_h donates the wind speed at hub height.

After reaching the rated wind speed, the electrical power output remains at its rated power in phase III. Sustained high wind speeds could lead to intense fatigue and extreme loads for the wind turbine generator system. Therefore, the rotor blades are automatically adjusted to the respective wind speed, when the wind speed reaches or exceeds the rated speed. This adjustment is intended to limit the power output by means of appropriate different strategies, which typically include stall and pitch regulation controls [25], in order to prevent exceeding the rated generator power.

In phase IV, when the wind speed exceeds the secured maximum wind speed value, the wind turbine is switched off. Even at extremely high wind speeds, no electrical power is generated, and the cut-off wind speed is approx. 20–25 m/s.

2.1.2 Modelling of regional aggregated wind power characteristic

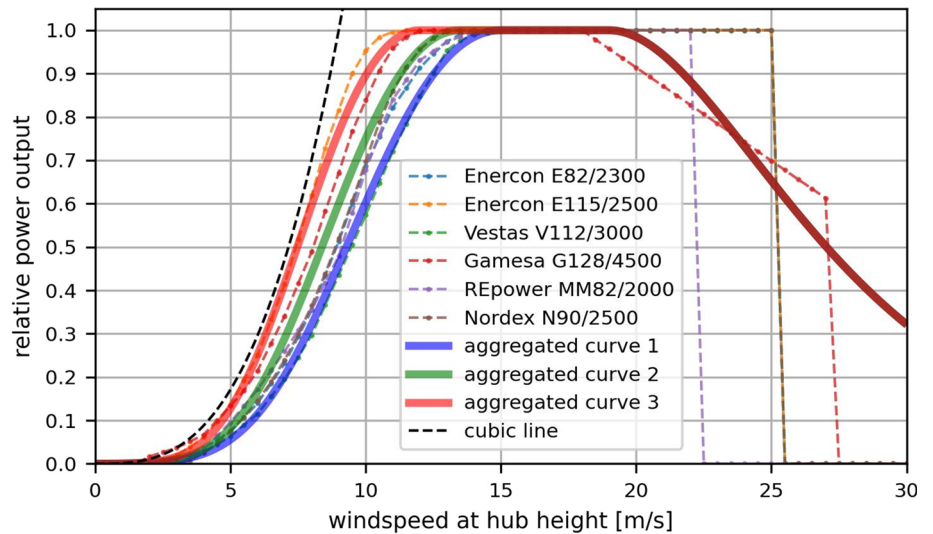
The regional wind power output is actually aggregated from different wind power plants (WPPs). They have various characteristic curves, inclusive cut-in, cut-out speed and slope of power increase. One single wind turbine power curve is not sufficient for the regional power output prediction.

Figure 2 shows the different characteristic curves of WT. The power performance in phase II varies for different manufacturers and turbine types. Furthermore, with new technology development in WT, such as optimized blade geometry, increased rotor diameter, improved starting characteristics, and enhanced electrical efficiency and so on, the so-called low speed WT can also be applied in areas with low wind conditions [27]. These low-speed wind turbines yield high wind power, especially at low and medium wind speeds, due to their higher power efficiency. For a typical low-speed WT (i.e. Enercon E115/2500) with a wind speed of 10 m/s, the relative power output can reach over 90%. In contrast, a standard WT (i.e. Enercon E82/2300) can only obtain about 60% of rated power with a wind speed of 10 m/s. As a result, standard wind turbines have lower full load hours and average energy yield compared to low-speed wind turbines.

In addition to considering phase II, the switch-off stage in phase IV must also be taken into account. Different cut-out wind speeds and stepwise switch-off processes are illustrated in Fig. 2. The characteristic curves of regional different wind turbines can be smoothed and combined into one regional aggregated characteristic curve.

Due to different ageing and types of WTs, three types of aggregated curves were used to represent WTs installed at different times. The status of installed capacity until the end of the year 2019 is analysed in this work. Aggregated curve 1 represents the WTs from 15 years ago with a relatively lower power characteristic (i.e. Enercon E82/2300).

Fig. 2 Regional aggregated wind power characteristics



Aggregated curve 3 represents the WT’s from the last 5 years with a relatively higher power characteristic (i.e. Enercon E115/2500). A third aggregated curve is generated for the years in between. The three aggregated power curves account for the fact that different technologies are used over the years. According to the three aggregated characteristic curves, the relative wind power outputs at a wind speed of 10 m/s at hub height are approx. 60%, 75% and 90%, respectively.

The Gumbel distribution is widely used in determination of extreme wind values distribution [28–30]. In this work, we used the scaled Gumbel distribution function to simulate the regional aggregated wind power characteristic curve. The Probability Density Function (PDF) of the Gumbel distribution is as follows:

$$g(x; \mu, \beta) = \frac{1}{\beta} * \exp\left(-\frac{x - \mu}{\beta}\right) * \exp\left[-\exp\left(-\frac{x - \mu}{\beta}\right)\right] \tag{2}$$

where μ is the location parameter, β is the scale parameter.

So after setting the values of the location and scale parameters of the Gumbel distribution function, the maximum values will be calculated. The maximum value of PDF should be scaled to 1, which corresponds to the maximal relative power output with a value of 1. Then the scaling process with max value can be described as follows:

$$g_{\text{scaled}}(x; \mu, \beta) = \frac{g(x; \mu, \beta)}{g_{\text{max}}(x; \mu, \beta)} \tag{3}$$

The scaled Gumbel distribution function is applied for the phase II and phase IV (as shown in Fig. 2). The aggregated switch-off phase uses the shifted descending stage of the scaled Gumbel distribution function. The hybrid distribution

function is defined and applied in different intervals:

$$p_{\text{relative}}(v_h) = \frac{P_{\text{WT, model}}}{P_{\text{wind, inst}}} = \begin{cases} 0 & \text{(for } v_h \text{ in phase I)} \\ g_{\text{scaled}}(v_h; \mu, \beta) & \text{(for } v_h \text{ in phase II)} \\ 1 & \text{(for } v_h \text{ in phase III)} \\ g_{\text{scaled}}((v_h - \Delta\mu); \mu, \beta) & \text{(for } v_h \text{ in phase IV)} \end{cases} \tag{4}$$

where p_{relative} is the relative power with respect to the installed capacity ($P_{\text{wind, inst}}$), $\Delta\mu$ is the shifted value. It is determined from the cut-out wind speed v_{out} and rated wind speed v_{rated} .

$$\Delta\mu = v_{\text{out}} - v_{\text{rated}} \tag{5}$$

Through hyper parameter optimization of μ and β for typical power characteristics of standard WT and low-speed WT, the specific parameters for the aggregated power characteristic are set as follows:

During the wind power conversion process, wind speed is used as input data. In order to reduce the discrepancy between different weather measurements stations, the clustered mean wind speeds are used. Subsequently, the measured ground wind speed (at 10 m high) need to be converted to the specific hub height of the turbines, as the wind speed is strongly dependent on the height. Using the hybrid distribution function of Eq. (4) and parameters setting in Table 1, the regional relative wind power output is calculated. By pre-processing the missing data and error data are detected and filtered for the measured data. They are then filled through multi-linear regression with data from the neighbouring measurement stations. The multi-linear regression method is found in [31].

Table 1 Parameters for aggregated characteristics

| | Parameters [m/s] | Assumption for the WPPs |
|--------------------|--|---------------------------|
| Aggregated curve 1 | $\mu = v_{\text{rated}} = 15;$ $\beta = 5.8; v_{\text{in}} = 2;$ $v_{\text{out}} = 19$ | Group 1 (G1: ~ 2005) |
| Aggregated curve 2 | $\mu = v_{\text{rated}} = 13.5;$ $\beta = 5.2; v_{\text{in}} = 2;$ $v_{\text{out}} = 19$ | Group 2 (G2: 2005 ~ 2015) |
| Aggregated curve 3 | $\mu = v_{\text{rated}} = 12;$ $\beta = 4.6; v_{\text{in}} = 2;$ $v_{\text{out}} = 19$ | Group 3 (G3: 2015 ~) |

The detailed implementation of multi-linear-regression pre-processing for wind speeds, and neighbours of the observed weather stations have been appended to the supplementary file.

The most commonly used simplified expression for the wind speed at a height of h is the Hellmann exponential law [32]. The wind speed at any height can be approximately determined based on a measured wind speed at a certain height. It expresses the correlation of the wind speed at two different heights and is expressed as:

$$\frac{v_2}{v_1} = \left(\frac{h_2}{h_1}\right)^\alpha \tag{6}$$

So the speed at height h based on the wind speed at height 10 m is given by:

$$v_h = v_{10} * \left(\frac{h}{10}\right)^\alpha \tag{7}$$

where α is Hellmann exponent, h is considered height, v_h and v_{10} are the desired wind speed at height of h and the measured wind speed in 10m high, respectively.

According to the ground roughness, different exponent values are adopted. An approximate value of 0.28 for the exponent would be appropriate in this work for terrain with small obstacles up to 15m (i.e. forests, settlements and small cities, etc.) [32].

In summary, the regional wind power estimation process based on the aggregated model is illustrated in Fig. 3. The allocation of regional wind power is presented in subsection Data and Regional Cluster. After the classification of each WT into different clusters and ageing groups the cluster wind power is calculated. Accordingly, the regional power is aggregated from each cluster. The comprehensive implementation details of python scripts used to achieve the regional aggregated model and pre-process wind speed data have been appended to the supplementary file.

2.2 Artificial neural networks

In addition to the proposed aggregated model, we have established artificial neural networks for the application of regional large-scale wind power estimation. For comparison purposes, we proposed three neural network structures. One is simple LSTM model, one is stacked LSTM model, and the last one is a combined CNN–LSTM model.

2.2.1 LSTM and stacked LSTM model

The LSTM neural computation, a type of recurrent neural network (RNN), is first introduced by Hochreiter and Schmidhuber [33]. The LSTM addresses the challenge of long-term dependence and the vanishing gradient problem encountered by standard RNN models. The most significant contribution of LSTM is that it incorporates memory cells and gates to effectively handle information flow and retain information over extended periods. Therefore, it is possible to efficiently process time series data and capture their internal dynamic dependencies.

The architecture of an LSTM network consists of memory blocks known as cells, each with a cell state and a hidden state. These cells play a crucial role in making important decisions by storing and discarding information using gate mechanisms, including forget gate, input gate, and output gate [34]. Figure 4 illustrates the standard architecture of RNN and LSTM. The forget gate is utilized to determine which information should be forgotten or retained in the cell state. This involves processing the current time step input $x(t)$ and the previous hidden state value $h(t - 1)$ using the sigmoid function. The calculation for the forget gate is as follows:

$$f(t) = \text{sig } m(W_f \cdot [h(t - 1), x(t)] + b_f) \tag{8}$$

In the second phase of the calculation, the network progresses by transforming the previous cell state $C(t - 1)$ into a new cell state $C(t)$. This step determines the new information that needs to be incorporated into the long-term memory (cell state). To obtain the updated cell state value, the calculation considers the reference values from the forget gate, input gate and cell update gate. The formulas for this process are presented as follows:

$$i(t) = \text{sig } m(W_i \cdot [h(t - 1), x(t)] + b_i) \tag{9}$$

$$C'(t) = \tan h(W_c \cdot [h(t - 1), x(t)] + b_c) \tag{10}$$

$$C(t) = C(t - 1) \cdot f(t) + i(t) \cdot C'(t) \tag{11}$$

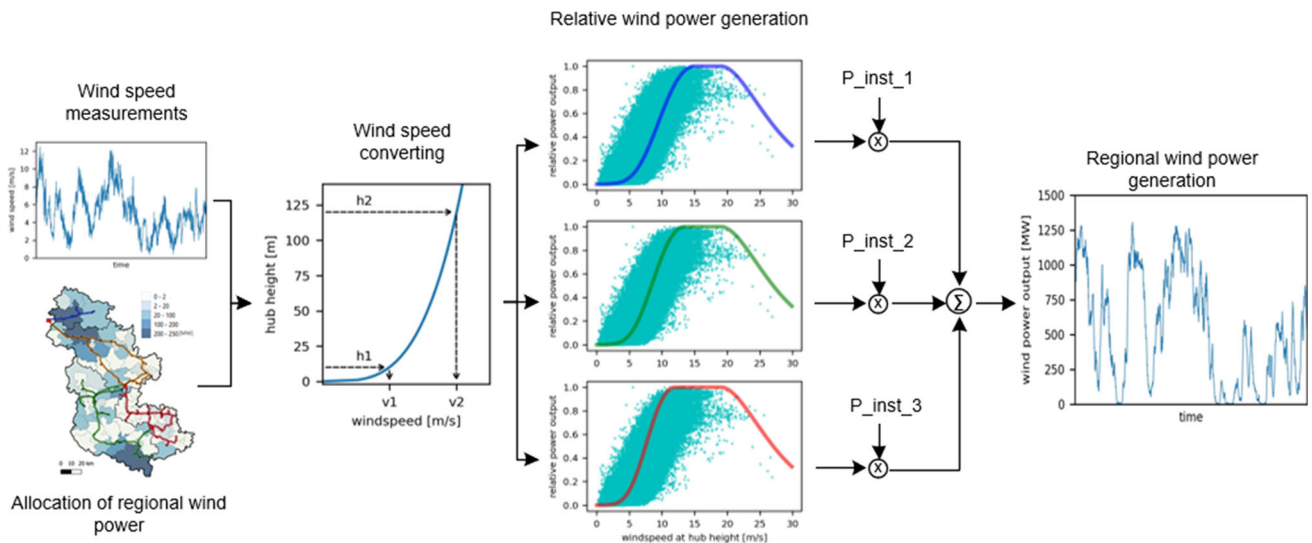


Fig. 3 The procedure of regional wind power generation calculation

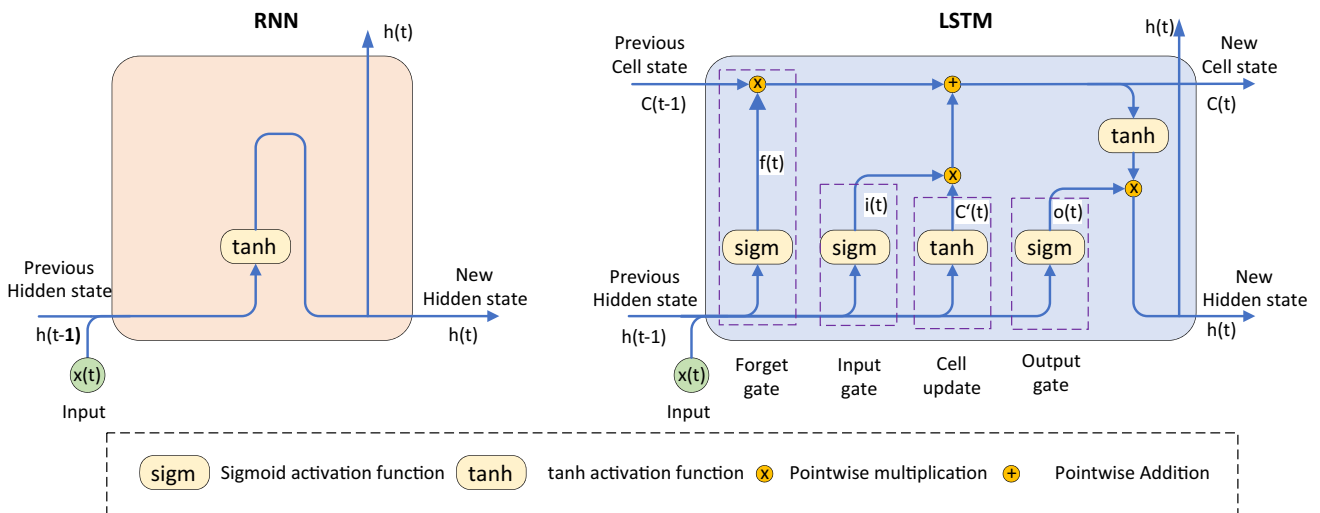


Fig. 4 Standard architecture of RNN and LSTM models

After updating the cell state, the next step involves determining the value of the hidden state $h(t)$. The hidden state serves as the network’s memory, retaining information from previous data to aid in making predictions. To calculate the hidden state, the process relies on the updated cell state and output gate $o(t)$. The formula for this step is provided as follows:.

$$o(t) = \text{sig } m(W_o \cdot [h(t - 1), x(t)] + b_o) \tag{12}$$

$$h(t) = o(t) \cdot \text{tanh}(C(t)) \tag{13}$$

Figure 5 shows the structures of LSTM and stacked LSTM, where the input layer receives the time sequential data, hidden layer computes with LSTM blocks and output

layer returns the result. Stacked LSTM model has more hidden layers with LSTM. As shown in Fig. 6, the past wind speed measurements (look back window) can be treated as a whole input. $X_n(t)$ donates the input feature at time t , such as measured wind speed from one measurement site n .

2.2.2 CNN–LSTM model

The Convolutional Neural Networks (CNN) is one kind of feed-forward neural networks that include convolutional computations with a deep structure. The CNN was firstly developed for image recognizing and processing [20]. An essential benefit of CNN is their ability to use convolutions filter and max-pooling layer to reduce the dimensions of the input data [20].

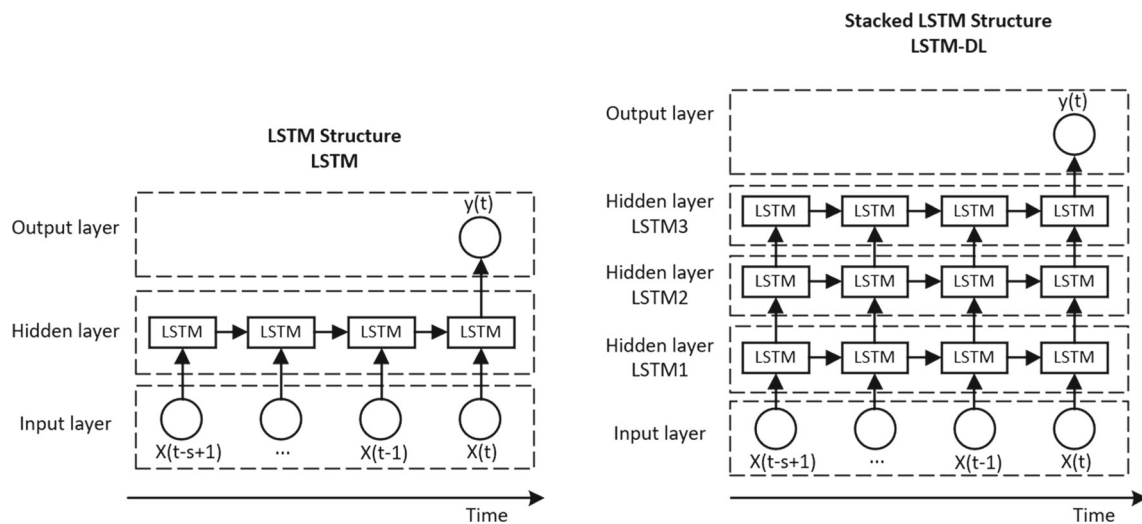


Fig. 5 LSTM and stacked LSTM deep structures

Fig. 6 Structure of the input features and output target

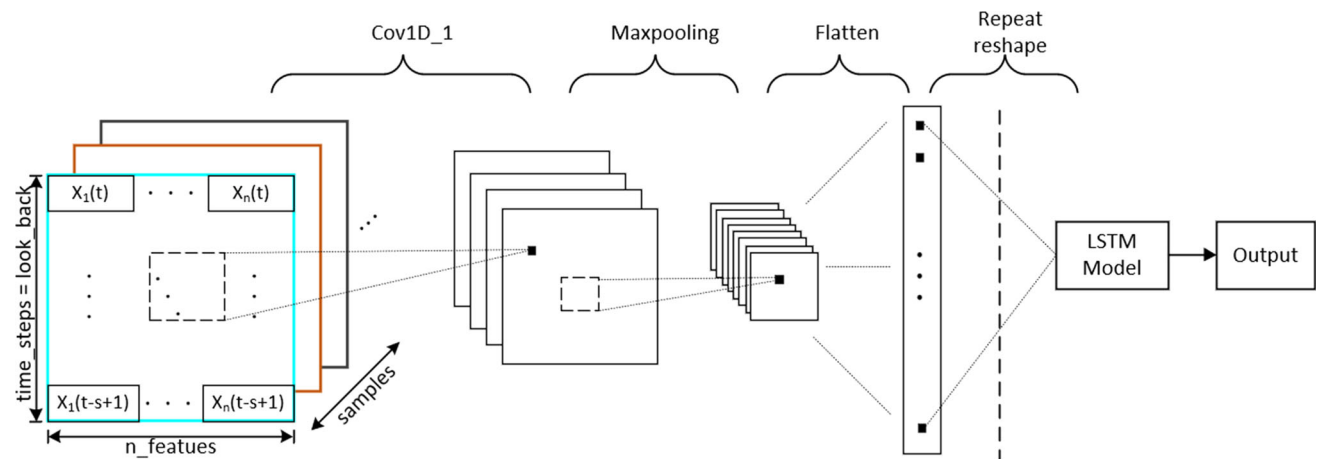
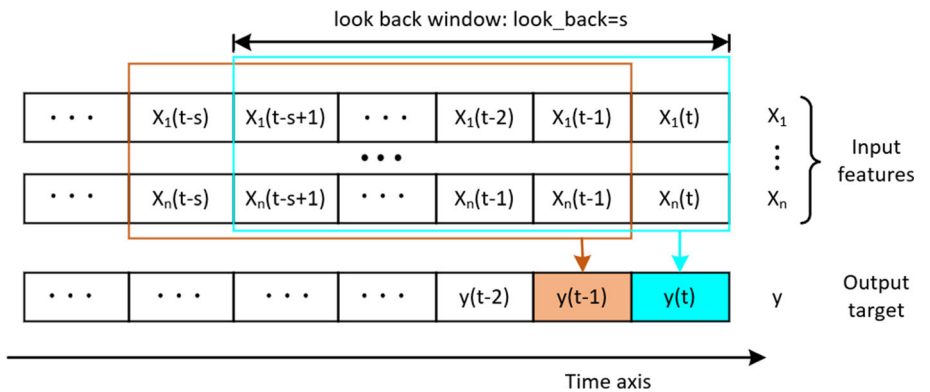


Fig. 7 CNN-LSTM structure

In this paper, we used a merged CNN–LSTM architecture (Fig. 7) for regional wind power prediction. The time sequential data from different features are used to construct a block map, resembling a feature image. The resulting 3D data structure feature maps can be received and viewed by CNN model recognition. After a range of CNN treatments, such as convolution, maxpooling and flatten, the output vector is reshaped and serves as the input for the LSTM model.

2.2.3 Parameters for neural networks

One step of input features with a matrix of [time_steps, n_features] is set as one input shape. It should be noted that the parameter “time_steps” actually corresponds to the size of look back window. In this work, we defined four different look back steps to test different look back window sizes of historical data for the current wind power estimation. In particular, the values of look back window size were set to $s = 12, 24, 48, 96$, which correspond to the last 3, 6, 12, 24 h due to 15 min time resolution.

Wind power generation often exhibits seasonal variations due to factors such as changes in weather patterns, atmospheric conditions, and regional climate. Wind speed and consequently wind power can also display daily patterns, influenced by factors like diurnal temperature and local wind patterns. Including seasonal and daily features, such as season indicators and time of day indicators, allow the LSTM model to capture these recurring pattern, enhancing the prediction accuracy for specific time intervals. Therefore, we added another four parameters to store the daily and seasonal features, namely $[\cos(2\pi \frac{t}{TD}), \sin(2\pi \frac{t}{TD})]$ and $[\cos(2\pi \frac{t}{TA}), \sin(2\pi \frac{t}{TA})]$. Since the temporal resolution is 15 min, each day contains 96 time series data points, there are a total of 35,040 time series data points for one year. Therefore, the periods of TD and TA are 96 and 35,040, respectively. The input features consist of multivariable wind speeds from different measurement stations (14 sites) and four daily and seasonally features form, resulting in a total of 18 input features.

The other parameter setups for the neural networks are listed in Table 2. In this paper the neural network components and structures are built using TensorFlow, which is a free and open-source machine learning and artificial intelligence platform [35]. To prevent overfitting, an EarlyStopping function with patience of 3 is utilized and the training epochs is set as 10. The detailed neural network configurations can be found in the implemented program code of python scripts in the supplementary file.

2.3 Data and regional cluster

The evaluation of regional wind power is based on the regional aggregated installed capacity. The master data for

Table 2 Parameters for neural networks

| Model | Parameters setup |
|----------|--|
| LSTM | LSTM(units = 10) → Dense(units = 1) activation = 'relu'; optimizer = 'Adam' |
| LSTM-DL | LSTM(units = 10) → LSTM(units = 10) → LSTM(units = 10) → dense(units = 1) activation = 'relu'; optimizer = 'Adam' |
| CNN–LSTM | Conv1D(filters = 10, kernel_size = 3) → Cov1D(filters = 10, kernel_size = 3) → MaxPooling1D(pool_size = 2) → Flatten() → LSTM(units = 10) → LSTM(units = 10) → Dense(units = 1) activation = 'relu'; optimizer = 'Adam' |

renewable energy sources annual statement are published by the Transmission System Operators (TSO) [36]. In addition, the market master data register (MaStR, German: Marktstammdatenregister) is the register for the German electricity and gas market. All new electricity generation plants must be registered in MaStR from [37], which is managed by the Federal Network Agency (BNetzA, German: Bundesnetzagentur). These data contain the postal code of all RE sources systems, which can be used to detect their locations. The real regional wind power infeed data were provided by a local DSO. Due to the inhomogeneous distribution of RE installations and supply areas, we have divided the investigated region into four clusters based on our previous work in [21]. The details of the regional installed wind turbines, along with their postal code assignments to clusters, are provided in the supplementary file.

The allocation of installed WTs in north-eastern German subnet is illustrated in Fig. 8 for each postal code area. Totally 14 wind speed measurement stations with individual station ID are illustrated in Fig. 8 as well. The wind speed data are obtained from the German Weather Service (DWD, German: Deutscher Wetterdienst), which offers access to the Climate Data Centre portal with a wide range of climate data [38]. The historical regional observed wind speeds from weather measurement stations, and the historical regional wind power generation data have been included in the supplementary file.

According to the installation date the regional over 1000 WTs are further divided into 3 groups. Among them, there are about 115 new installed WTs after the year 2015. Compared to the installed rated power of WTs before 2005, the mean new installed capacity of a single WT has been almost tripled. Furthermore, the mean hub height has increased from around 75 m for WTs installed before 2005 and 136 m for the WTs installed after 2015. Overall, across the region, approx. 1721 MW of wind energy capacity had been installed by the end of the year 2019 (Fig. 9).

Figure 10 displays the scatter matrix with correlation coefficients of the data, consisting of regional normalized wind

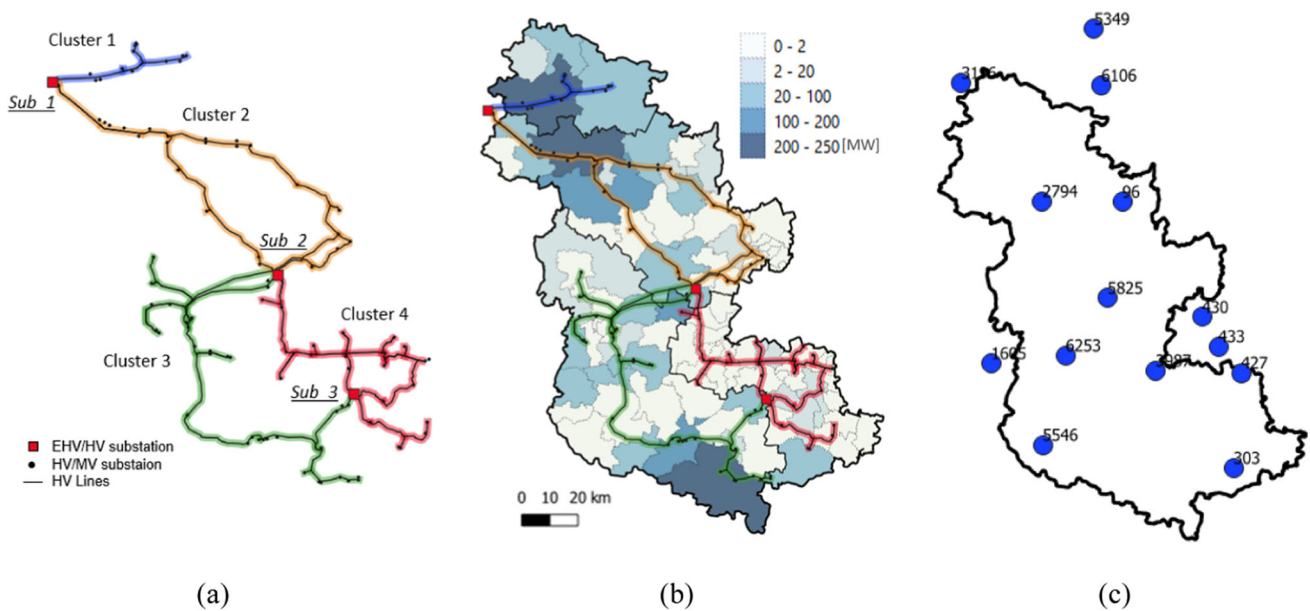


Fig. 8 Allocation of regional clusters (a) and installed wind capacity (b) and regional wind speed measurement stations with ID (c) (based on [21])

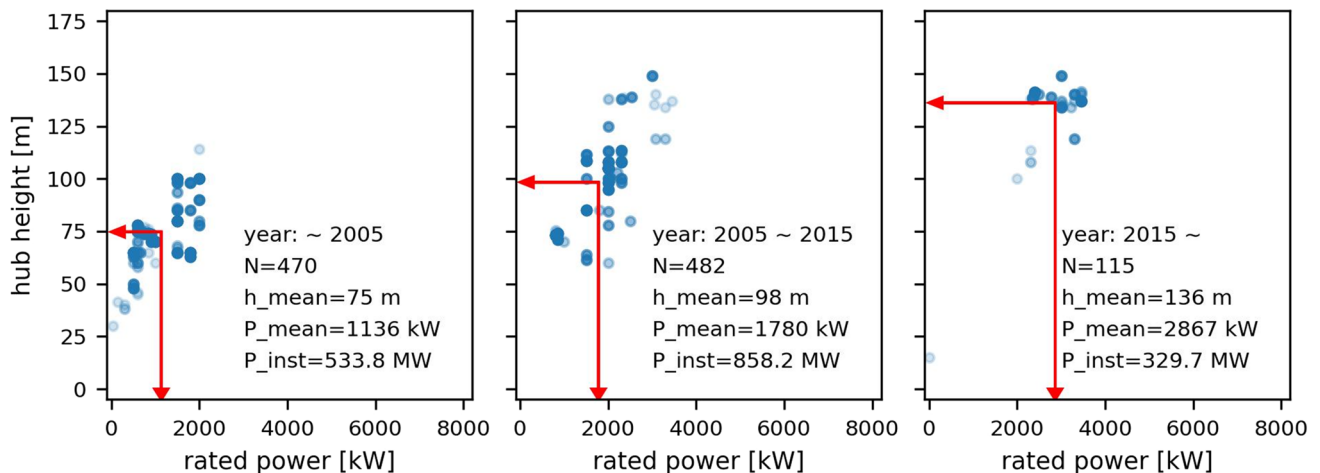


Fig. 9 The mean installed capacity and hub height for one region

power relative to installed capacity and regional wind speed from selected measurements sites. The correlation matrix is computed using the Pearson correlation coefficient, which quantifies the strength of the linear relationship between pairs of observed variables [21]. It is evident that the correlation coefficients between wind speeds and wind power range from 0.68 and 0.75, indicating a moderate linear association. However, this does not fully capture the complex and nonlinear nature of the relationship between wind power and wind speed in reality.

2.4 Performance metrics

In this study, we employ the following five performance metrics, namely mean absolute error (MAE), root mean squared

error (RMSE), relative mean absolute error (rMAE), relative root mean squared error (rRMSE), and full-load hours (FLH), to comprehensively evaluate the estimated wind power using the proposed methodology of aggregated model and neural network models. MAE represents the average absolute error between the actual and predicted values [17]. Mathematically, MAE can be expressed as:

$$MAE = \frac{1}{N} \sum_{i=1}^N |P_{pred} - P_{true}| \tag{14}$$

where P_{pred} donates the estimated power, P_{true} donates the original real power, and N donates the sample size of observation period. RMSE provides an overall measure of

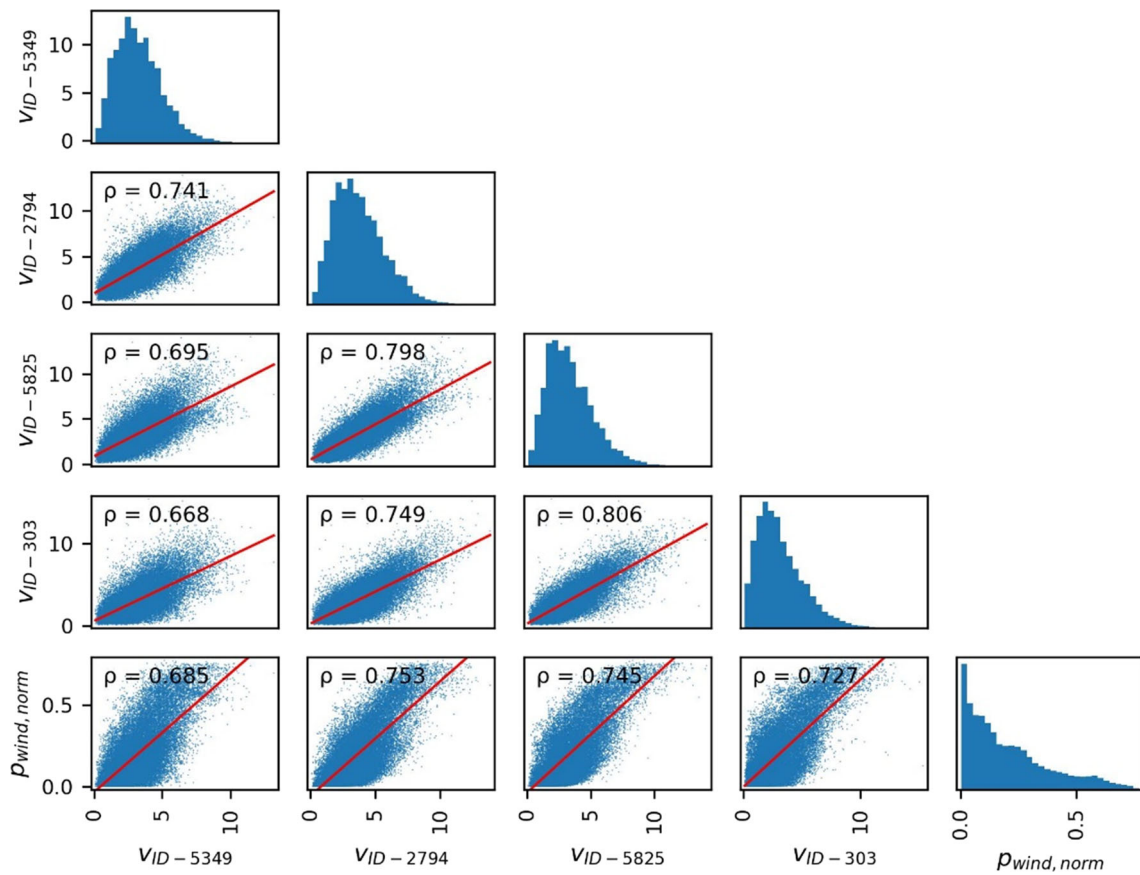


Fig. 10 Scatter matrix and correlation matrix of selected data

agreement between the estimated and original data, while preserving the performance in the original units by taking the square root of mean squared error [17]. It is defined as:

$$RMSE = \sqrt{\frac{1}{N} \sum_{i=1}^N (P_{pred} - P_{true})^2} \tag{15}$$

In addition, rMAE and rRMSE provide a relative measure of the prediction error and is normalized by the rated installed capacity, taking into account the scale of the data.

$$rMAE = \frac{1}{N} \sum_{i=1}^N \frac{|P_{pred} - P_{true}|}{P_{inst}} \tag{16}$$

$$rRMSE = \sqrt{\frac{1}{N} \sum_{i=1}^N \left(\frac{P_{pred} - P_{true}}{P_{inst}} \right)^2} \tag{17}$$

The desired values for MAE, rMAE, RMSE, rRMSE are zero, indicating a perfect model with no prediction error. A lower value indicates better performance.

Additionally, full-load hours is a metric that measures the actual operating time of a power generation source, typically

a renewable energy source like wind turbines, at its maximum rated capacity during a specific period, typically a year [39]. However, in reality, wind turbines do not always operate at their maximum capacity due to variations in wind speed. The metric of FLH reflects the efficiency and utilization of the power source by indicating how much of its potential capacity is being utilized.

$$FLH = \frac{\sum_{i=1}^N (P * \Delta t)}{P_{inst}} \tag{18}$$

where P donates the generated electrical power, Δt donates the time duration, and P_{inst} donates the rated installed capacity.

3 Results and discussion

In this section, we conducted tests on the proposed aggregated wind power curves for different wind turbines in the clustered areas. Figures 11 and 12 illustrate the clustered wind installed capacity and the mean hub height for different ageing groups, respectively. By the end of 2019, cluster 1 has an installed wind capacity of 367 MW. Both cluster 2

Fig. 11 Clustered installed wind capacity for different ageing groups

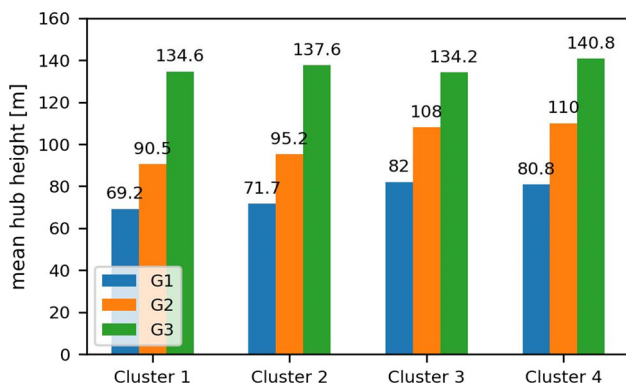
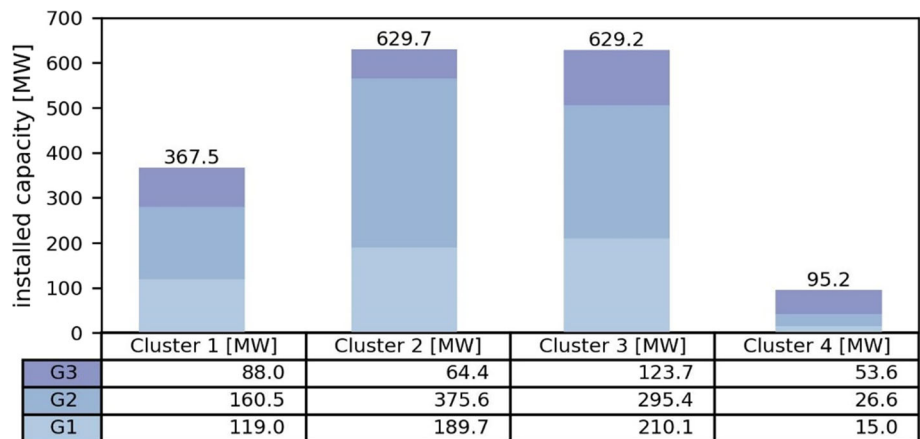


Fig. 12 Clustered mean hub height for different ageing groups

and 3 have about 629 MW installed capacity, whereas cluster 4 has a lower installed capacity of 95.2 MW. In terms of the mean hub height, all four clustered areas have an average hub height above 130m for the ageing group G3.

The wind speeds obtained from different measurement stations serve as input parameters. The clustered wind power is then calculated based on the classification process and the converting procedure shown in Fig. 3. Figure 13 illustrates the modelled wind power results for the four clusters. It can be observed that the modelled wind power accurately captures the changes and exhibits peak power generation during certain time periods. Although cluster 2 and cluster 3 have similar wind power installed capacity, their power characteristics and weather conditions differ, leading to variations in their power generation profiles. In addition, since cluster 4 has the highest mean hub height, it reaches its rated power quickly and maintains it for a longer duration.

However, there is a significant difference in peak power between the regional aggregated wind power and the real measured wind power. As shown in Fig. 14, the average relative peak power, based on the real measured data with reference to installed capacity, varies monthly. The preliminary modelled wind power results can reach its rated power

almost every month. The real mean wind peak power can only range between approx. 55% in summer and 80% in winter.

Such large power differences are attributed to the fact that the preliminary aggregated model does not take the actual operating situation into account. The correction factor may include the following influencing aspects. Firstly, some wind power generation systems may be unavailable due to the planned and unplanned maintenance and repair work. Additionally, the wind turbine generators cannot operate strictly along their characteristic curves due to the different local wind strength and wind directions in terms of the day and seasons. The rotor direction of the wind turbine must be adjusted accordingly, which results in electrical self-consumption and a delay in fully utilizing the available wind speed for electricity generation.

Furthermore, there are inefficiencies in the start-up process at lower wind speeds, and the presence of turbulence results in significant losses during the generation process. Moreover, the wind generators are not directly installed near the connection point of the electricity grid network. The generated wind power needs to be transferred through cables to the connection point and transformed to the appropriate voltage levels, which inevitably leads to power losses during the transfer and transformation.

In addition to the mentioned technical factors, there are some requirements for switch-off or curtailment at certain time of the days and seasons. For the reason of congestion management and grid capacity, the current grid may not be able to absorb the generated electrical energy. In this case, the excess electricity generation cannot be fed into the grid.

Therefore, the new regional wind power ($P_{WT, model}^*$) can be expressed using the correction factor as follows:

$$P_{WT, model}^* = P_{WT, model} * f_c \tag{19}$$

The dynamic correction factor is monthly updated through an investigation of the historical data. The correction factor is calculated based on the multiple relationship between the

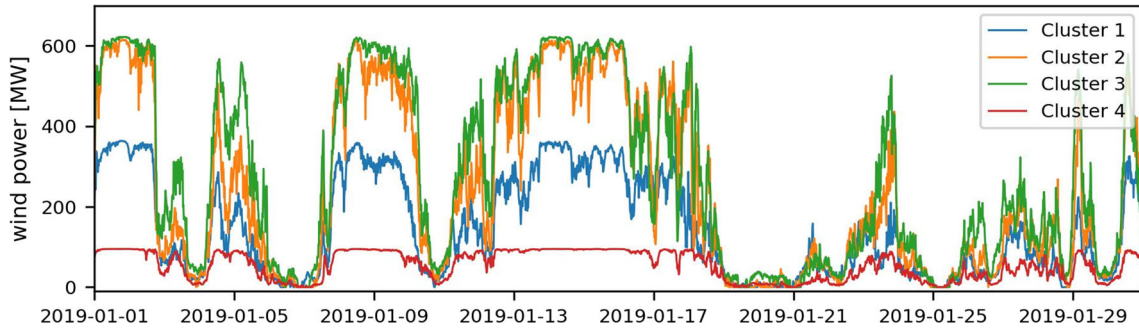
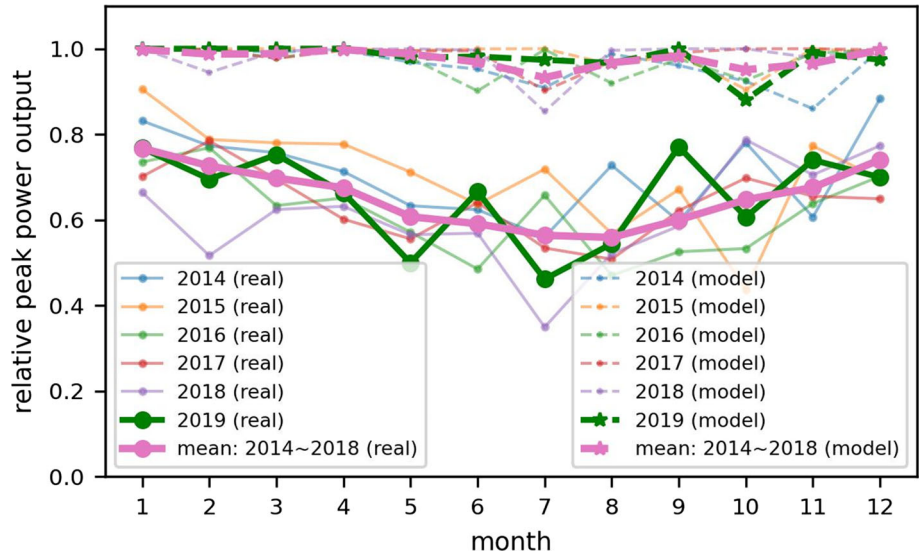


Fig. 13 Modelled clustered wind power

Fig. 14 Monthly relative peak power output



mean measured peak power from previous years and the corresponding mean modelled peak power (as shown in Fig. 14). The definition of the correction factor is as follows:

$$f_c(m) = \frac{\frac{1}{Y} \sum_{i=1}^Y P_{\text{peak},i}^{\text{measure}}(m)}{\frac{1}{Y} \sum_{i=1}^Y P_{\text{peak},i}^{\text{model}}(m)} \quad (20)$$

where f_c donates the monthly dynamic correction factor including all influencing factors, $P_{\text{peak},i}^{\text{measure}}(m)$ donates measured peak power relative to the installed capacity in month m of year i , while $P_{\text{peak},i}^{\text{model}}(m)$ donates the relative peak power calculated by aggregated model.

As shown in Fig. 15, the new regional aggregated wind power is plotted. The preliminary modelled wind power (represented by the blue dashed line) exhibits a higher peak power output compared to the real measured (represented by the red line). In order to adjust the peak power of the model we applied a correction factor. By analysing the historical data from the past five years, we apply a correction factor of 76.9% for January to align the modelled results. The correction factors are statistically examined using the historical mean values from the years 2014 to 2018 (as shown Fig. 14).

The new corrected power curve (represented by the orange dashed line) demonstrates that the new aggregated model with the inclusion of the correction factor can accurately predict the regional real wind power.

After applying the historical dynamic correction factor f_c on the modelled regional wind power, the metrics of the proposed model are to be evaluated. The metrics, including Mean absolute error (MAE), root mean squared error (RMSE), relative mean absolute error (rMAE) and relative root mean squared error (rRMSE) with reference to the rated power are calculated and presented in the following Table 3. The metric values are calculated based on the entire year 2019. It is noticeable that a significant improvement was achieved for the aggregated model with correction factor for different performance evaluations. The annual prediction error of rMAE can reach around 8.4%.

As comparison we examine the neural network models. After pre-processing of the measured data with different look back windows we randomly split the data into training and validation datasets based on the data of the year 2018. After the model is trained we use the year 2019 data as test dataset

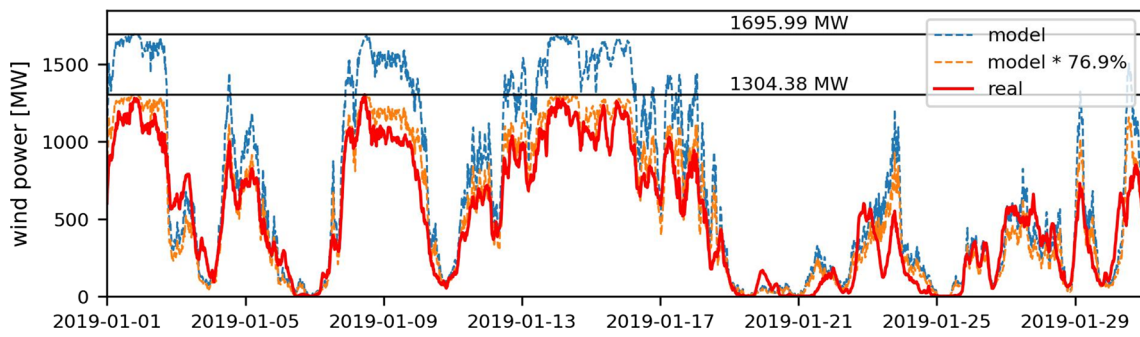


Fig. 15 Regional aggregated wind power

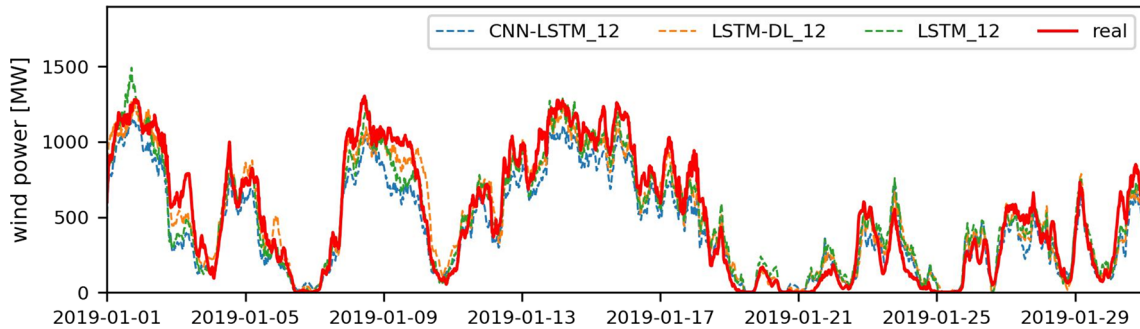


Fig. 16 Wind power estimation based on different neural network models

Table 3 Evaluation of metrics for the modelled wind power for the year 2019

| | Model without correction factor ($P_{WT,model}$) | Model with correction factor ($P_{WT,model}^*$) |
|-----------|--|---|
| MAE | 237.3 MW | 143.1 MW |
| RMSE | 320.8 MW | 185.7 MW |
| rMAE (%) | 13.8 | 8.4 |
| rRMSE (%) | 18.6 | 10.9 |

for the regional power prediction. Figure 16 shows the predicted regional wind power based on different neural network models with look back window of $s = 12$ (equivalent to 3 h). All the three neural network models successfully capture the variations in regional wind power based on the regional distributed wind speed measurement.

In addition, Fig. 17 shows the monthly comparisons from all tested models with different look back windows. It can be seen that the neural network models outperform the aggregated model in terms of prediction performance. Meanwhile, the metric of rMAE exhibit lower prediction errors during the summer months compared to the winter months. Notably, LSTM-DL achieves an rMAE of approx. 3% from June to August and about 6% during winter.

Figure 17 also presents the annual evaluation of rRMSE. LSTM-DL consistently demonstrates excellent performance

across different look back window sizes. LSTM also exhibits strong predictive capabilities with a look back window of either 3 h ($s = 12$) or 24 h ($s = 96$). Relatively, CNN-LSTM model does not perform as well as LSTM and LSTM-DL model. It may need more epochs for training process because of more weighting parameters and convolutional computation.

Furthermore, we investigated and compared the annual duration curve for the modelled regional wind power. As shown in Fig. 18, the annual duration curve of the corrected model power is close to the actual duration curve. Concerning the full load hours (FLH), the real measured wind power generation in the investigated region has 1794 FLH for the year 2019. The aggregated model has approx. 1638 FLH with a deviation of 156 h to the real measurement. Overall, the annual duration curve form LSTM-DL model close better to the real measurement. The peak power reach about 80% of the rated power.

Additionally, Table 4 shows the FLH difference between real measurement and the prediction results based on deep learning models with a various look back window sizes. LSTM and LSTM-DL perform better in predicting the FLH than CNN-LSTM and the aggregated model. The results indicate that the stacked deep learning model of LSTM-DL with a look back wind of the last 6 h ($s = 24$) performs the best, while the model with a look back wind of the last 24 h ($s = 96$) shows similar performance. The reason behind this similarity in performance could be attributed to the nature of

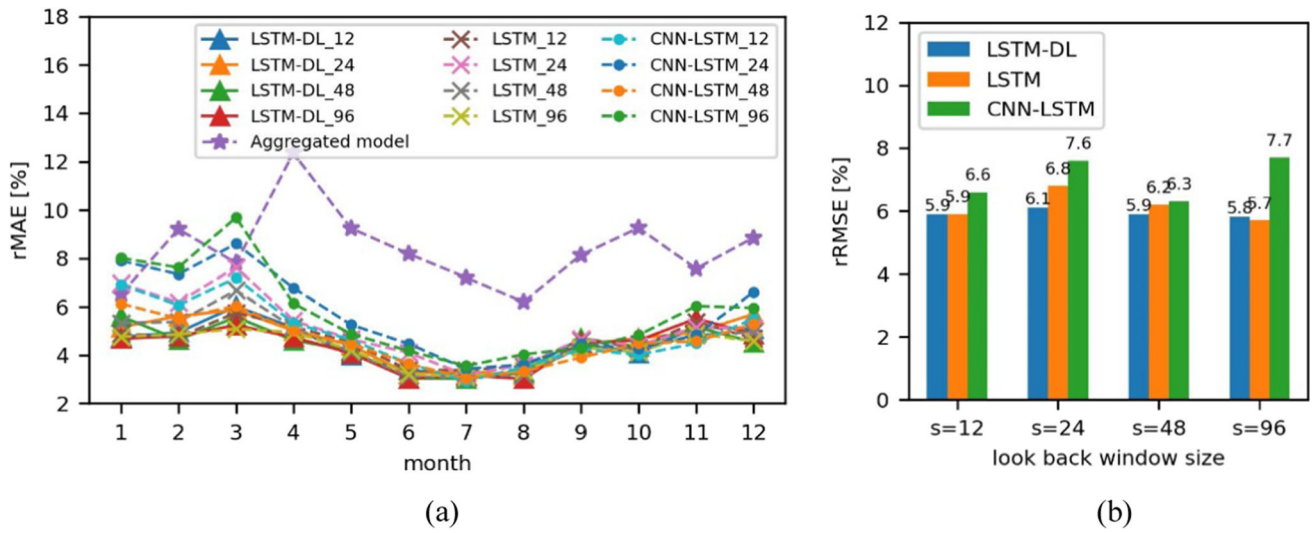


Fig. 17 Monthly rMAE (a) and annual rRMSE (b) of neural networks

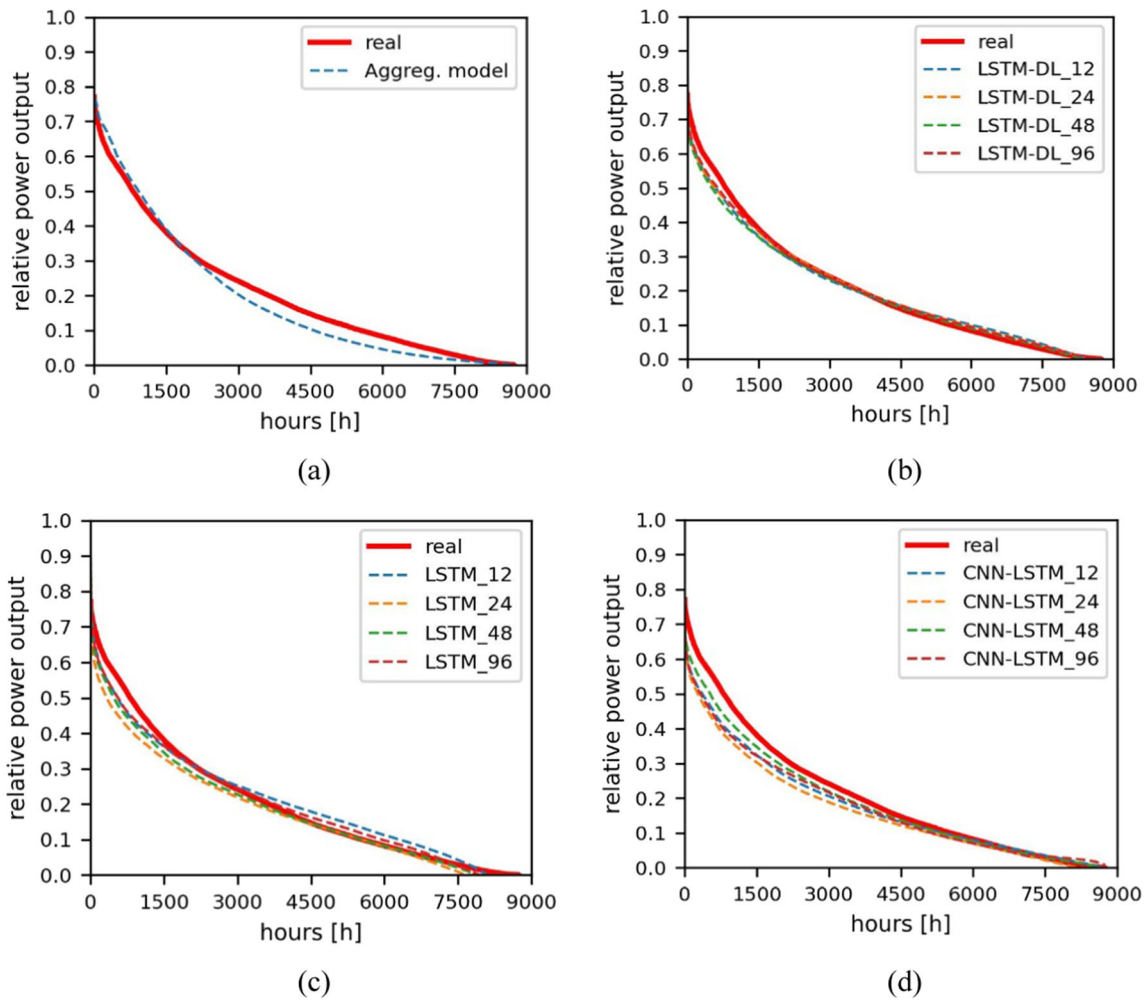


Fig. 18 Annual duration curve from different models for the year 2019

Table 4 FLH difference (in hours) between prediction and real situation

| Models | Look back | | | |
|----------|---------------------|---------------------|----------------------|----------------------|
| | $s = 12$ (last 3 h) | $s = 24$ (last 6 h) | $s = 48$ (last 12 h) | $s = 96$ (last 24 h) |
| LSTM-DL | 30 | 4 | 76 | 6 |
| LSTM | 51 | 228 | 148 | 21 |
| CNN-LSTM | 237 | 366 | 161 | 243 |

wind power generation. Wind power is influenced by various factors such as wind speed, wind direction, and atmospheric conditions. While the last 6 h ($s = 24$) of wind speeds capture recent changes and short-term patterns, the last 24 h ($s = 96$) provide a broader perspective and incorporate longer-term trends. The LSTM model is effective at learning temporal dependencies within a given time window. It is possible that the additional information from the last 6 h ($s = 24$) and last 12 h ($s = 48$) does not significantly contribute to the prediction accuracy beyond what is already captured by the last 3 h ($s = 12$) in the standard LSTM model. The LSTM model with a look back window of the last 24 h ($s = 96$) performs better compared to the other look back windows. This suggests that the LSTM model's memory cells enable it to retain information over longer time periods, which is beneficial for capturing longer-term patterns and trends in wind power data. However, it is evident that using smaller look back window size reduces the computational cost for the neural network. As the look back window increases, the size of the training parameter also grows exponentially, leading to a significant increase in computation requirements.

4 Conclusions

In this study, we proposed a novel model for the regional wind power estimation based on the characteristics of regional wind power. Three aggregated characteristic curves representing the synthetic curves of locally installed wind turbines at different time periods are used. While theoretically the investigated power characteristic curve can imitate the regional wind power output, it is important to consider that not all wind turbines are in operation and wind turbines cannot always operate optimally. Therefore, a dynamic correction factor is derived through the statistical analysis of historical regional wind power data to improve the prediction results. By using 15 min measured data from the local DSO, the power performance assessment is investigated. In addition, different neural networks with deep learning models are suggested in this paper. Essentially these proposed neural computations achieve good performance for the regional wind power estimation and prediction. The annual prediction error, measured by rRMSE, decreases from 10.9% to around 6%. Particularly, the monthly rMAE demonstrates

that, the neural networks achieves about 3% rMAE in summer and about 6% in winter. The wind power annual duration curve from real measurement and the deep learning model of LSTM-DL shows a strong match. The full-load hours differs only 4 h by using the last 6 h data for the prediction.

At the regional scale, we proposed clusters to analyse the allocation of wind power. The installed capacity of each postal code area is investigated to understand the regional development of wind power. The mean hub height of wind turbines in each cluster is statistically calculated. However, regional decentralized weather measurements do not directly represent the actual wind speed at hub height. The wind speed transformation process inevitably leads to errors for each cluster. A further limitation is that the real operating conditions of individual wind turbines during the year are very difficult to determine. For more accurate regional wind power prediction and estimation we recommend that more measurement sites can be used with corresponding spatial divisions. However, more data and small-scale divisions will require more computational cost, so a balance has to be found. An alternative option for comparison is to consider different classifications for each cluster. Artificial intelligence techniques, such as neural networks, can provide a solution to avoid the analysis of transformation processes. The internal mapping relations of input features can be trained and adjusted through self-learning. However, it is important to note that neural networks are often understood as black boxes, lacking explanatory power, and their complex structure may require more training epochs.

5 Competing interests

The authors declare that they have no known competing financial interests or personal relationships that could have appeared to influence the work reported in this paper.

Supplementary Information The online version contains supplementary material available at <https://doi.org/10.1007/s00202-023-02005-z>.

Authors' contributions: YL: Conceptualization; Methodology; Formal Analysis; Collection and Assembly of Data; Data Analysis and Interpretation; Writing—Original Draft; Writing—Review & Editing. PJ:

Supervision; Conceptualization; Methodology; Writing—Review & Editing. HS: Supervision.

Funding Open Access funding enabled and organized by Projekt DEAL.

Data availability The open data used to support the findings of this study are included within the article and also listed in references.

Declarations

Competing interests The authors declare no competing interests.

Open Access This article is licensed under a Creative Commons Attribution 4.0 International License, which permits use, sharing, adaptation, distribution and reproduction in any medium or format, as long as you give appropriate credit to the original author(s) and the source, provide a link to the Creative Commons licence, and indicate if changes were made. The images or other third party material in this article are included in the article's Creative Commons licence, unless indicated otherwise in a credit line to the material. If material is not included in the article's Creative Commons licence and your intended use is not permitted by statutory regulation or exceeds the permitted use, you will need to obtain permission directly from the copyright holder. To view a copy of this licence, visit <http://creativecommons.org/licenses/by/4.0/>.

References

1. Federal Ministry for Economic Affairs and Climate Action (BMWK) (2021) Renewable energy sources in figures National and International Development 2020. Berlin
2. Kuprat M, Bendig M, Pfeiffer K (2017) Possible role of power-to-heat and power-to-gas as flexible loads in German medium voltage networks. *Front Energy* 11:135–145. <https://doi.org/10.1007/s11708-017-0472-8>
3. Bundesnetzagentur (BNetzA) (2022) Monitoring Report 2021. Bonn
4. Majidi Nezhad M, Heydari A, Groppi D et al (2020) Wind source potential assessment using Sentinel 1 satellite and a new forecasting model based on machine learning: a case study Sardinia islands. *Renew Energy*. <https://doi.org/10.1016/j.renene.2020.03.148>
5. Foley AM, Leahy PG, Marvuglia A, McKeogh EJ (2012) Current methods and advances in forecasting of wind power generation. *Renew Energy* 37:1–8
6. Ren J, Yu Z, Gao G et al (2022) A CNN-LSTM-LightGBM based short-term wind power prediction method based on attention mechanism. *Energy Rep*. <https://doi.org/10.1016/j.egy.2022.02.206>
7. Chen Y, Wang Y, Dong Z et al (2021) 2-D regional short-term wind speed forecast based on CNN-LSTM deep learning model. *Energy Convers Manag*. <https://doi.org/10.1016/j.enconman.2021.114451>
8. Monforti F, Gonzalez-Aparicio I (2017) Comparing the impact of uncertainties on technical and meteorological parameters in wind power time series modelling in the European Union. *Appl Energy*. <https://doi.org/10.1016/j.apenergy.2017.08.217>
9. Song D, Yang Y, Zheng S et al (2020) New perspectives on maximum wind energy extraction of variable-speed wind turbines using previewed wind speeds. *Energy Convers Manag*. <https://doi.org/10.1016/j.enconman.2020.112496>
10. Liu H, Chen C, Lv X et al (2019) Deterministic wind energy forecasting: a review of intelligent predictors and auxiliary methods. *Energy Convers Manag* 195:328–345
11. Erdem E, Shi J (2011) ARMA based approaches for forecasting the tuple of wind speed and direction. *Appl Energy*. <https://doi.org/10.1016/j.apenergy.2010.10.031>
12. Hodge BM, Zeiler A, Brooks D, et al (2011) Improved wind power forecasting with ARIMA models
13. Liu X, Zhou J, Qian H (2021) Short-term wind power forecasting by stacked recurrent neural networks with parametric sine activation function. *Electr Power Syst Res*. <https://doi.org/10.1016/j.eprs.2020.107011>
14. Ouyang T, Zha X, Qin L (2017) A combined multivariate model for wind power prediction. *Energy Convers Manag* 144:361–373. <https://doi.org/10.1016/j.enconman.2017.04.077>
15. Pierro M, De Felice M, Maggioni E et al (2017) Data-driven upscaling methods for regional photovoltaic power estimation and forecast using satellite and numerical weather prediction data. *Sol Energy*. <https://doi.org/10.1016/j.solener.2017.09.068>
16. Abdel-Nasser M, Mahmoud K (2019) Accurate photovoltaic power forecasting models using deep LSTM-RNN. *Neural Comput Appl*. <https://doi.org/10.1007/s00521-017-3225-z>
17. Shahid F, Zameer A, Muneeb M (2021) A novel genetic LSTM model for wind power forecast. *Energy*. <https://doi.org/10.1016/j.energy.2021.120069>
18. Zhang H, Zhao L, Du Z (2021) Wind power prediction based on CNN-LSTM. In: 5th IEEE Conf Energy Internet Energy Syst Integr Energy Internet Carbon Neutrality, EI2 2021, pp 3097–3102. <https://doi.org/10.1109/EI252483.2021.9713238>
19. Chen X, Zhang X, Dong M et al (2021) Deep learning-based prediction of wind power for multi-turbines in a wind farm. *Front Energy Res*. <https://doi.org/10.3389/fenrg.2021.723775>
20. Agga A, Abbou A, Labbadi M et al (2022) CNN-LSTM: an efficient hybrid deep learning architecture for predicting short-term photovoltaic power production. *Electr Power Syst Res*. <https://doi.org/10.1016/j.eprs.2022.107908>
21. Li Y, Janik P, Schwarz H, Pfeiffer K (2022) Proposal of a regional grid cluster model for analysis of electrical power network performance. *Arch Electr Eng* 71:601–613. <https://doi.org/10.24425/ae.2022.141673>
22. Focken U, Lange M, Mönnich K et al (2002) Short-term prediction of the aggregated power output of wind farms—a statistical analysis of the reduction of the prediction error by spatial smoothing effects. *J Wind Eng Ind Aerodyn*. [https://doi.org/10.1016/S0167-6105\(01\)00222-7](https://doi.org/10.1016/S0167-6105(01)00222-7)
23. Saint-Drenan YM, Good GH, Braun M, Freisinger T (2016) Analysis of the uncertainty in the estimates of regional PV power generation evaluated with the upscaling method. *Sol Energy*. <https://doi.org/10.1016/j.solener.2016.05.052>
24. Hu W, Liu Z, Tan J (2020) Thermodynamic analysis of wind energy systems. In: Wind solar hybrid renewable energy system
25. Mohanpurkar M, Ramakumar RG (2010) Probability density functions for power output of Wind Electric Conversion Systems. In: IEEE PES general meeting, PES 2010
26. Xiao Z, Zhao Q, Yang X, Zhu AF (2020) A power performance online assessment method of a wind turbine based on the probabilistic area metric. *Appl Sci*. <https://doi.org/10.3390/app10093268>
27. Barnes RH, Morozov EV, Shankar K (2014) Improved methodology for design of low wind speed specific wind turbine blades. *Compos Struct*. <https://doi.org/10.1016/j.compstruct.2014.09.034>
28. Kang D, Ko K, Huh J (2015) Determination of extreme wind values using the Gumbel distribution. *Energy*. <https://doi.org/10.1016/j.energy.2015.03.126>
29. Shi H, Dong Z, Xiao N, Huang Q (2021) Wind speed distributions used in wind energy assessment: a review. *Front Energy Res* 9:769920
30. Ayuketang Arreyndip N, Joseph E (2016) Generalized extreme value distribution models for the assessment of seasonal wind

- energy potential of Debuncha. *Cameroon J Renew Energy*. <https://doi.org/10.1155/2016/9357812>
31. Suresh V, Janik P, Rezmer J, Leonowicz Z (2020) Forecasting solar PV output using convolutional neural networks with a sliding window algorithm. *Energies*. <https://doi.org/10.3390/en13030723>
 32. Reich G, Reppich M (2018) Nutzung der Windenergie. In: Reich G, Reppich M (eds) *Regenerative Energietechnik: Überblick über ausgewählte Technologien zur nachhaltigen Energieversorgung*. Springer Fachmedien Wiesbaden, Wiesbaden, pp 151–185
 33. Hochreiter S, Schmidhuber J (1997) Long short-term memory. *Neural Comput*. <https://doi.org/10.1162/neco.1997.9.8.1735>
 34. Aksan F, Li Y, Suresh V, Janik P (2023) CNN-LSTM vs. LSTM-CNN to predict power flow direction: a case study of the high-voltage subnet of Northeast Germany. *Sensors*. <https://doi.org/10.3390/s23020901>
 35. TensorFlow. <https://www.tensorflow.org/>. Accessed 16 Jul 2022
 36. Netztransparenz.DE EEG-Anlagenstammdaten. <https://www.netztransparenz.de/EEG/Anlagenstammdaten>. Accessed 16 May 2022
 37. Bundesnetzagentur (BNetzA) Market Master Data Register. <https://www.marktstammdatenregister.de/MaStR/>. Accessed 16 May 2022
 38. German Weather Service Climate Data Center. https://www.dwd.de/EN/climate_environment/cdc/cdc_node_en.html. Accessed 16 May 2022
 39. Pfaffel S, Faulstich S, Sheng S (2019) Recommended key performance indicators for operational management of wind turbines. In: *Journal of Physics: Conference Series*

Publisher's Note Springer Nature remains neutral with regard to jurisdictional claims in published maps and institutional affiliations.